An experimental investigation of sweeping jets impinging flow field: effects of nozzle-to-plate distance and feedback channel minimum cross-sectional area

Cristina D'Angelo[1,*], Carlo Salvatore Greco[1], Gerardo Paolillo[1], Gennaro Cardone[1], Tommaso Astarita[1]

1: Dept. of Industrial Engineering, University of Naples 'Federico II', Naples, Italy
*Corresponding author: cristina.dangelo@unina.it

Keywords: Sweeping jets, planar PIV, parametric analysis.

ABSTRACT

In the current work, the effects of the nozzle-to-plate distance and of the feedback channel minimum cross-sectional area on the external flow field of impinging sweeping jets are experimentally investigated through the application of the planar Particle Image Velocimetry (PIV) technique. Non-dimensional nozzle-to-plate distances H/w equal to $2, 4, 6, 8$ and 10 are taken into account, being w the exit nozzle throat section width. To analyse the effects of the feedback channel minimum cross-sectional area, a fluidic oscillator having a mixing chamber length $L_f/w = 4.5$ is provided with threaded holes in correspondence of the feedback channels, in which a micrometric screw is fastened to vary the parameter g/w, being g the feedback channel minimum passage width; values of g/w equal to $0.17, 0.33, 0.50, 0.67$ and 1 are considered. Time-averaged and phase-averaged analyses are performed in order to assess the effects of the parameters H/w and g/w on the external flow field of sweeping jets impinging on a flat plate. The obtained results show that, with the increase of the nozzle-to-plate distance, the jet no longer exhibits a rigid-like behaviour in its sweeping motion and the PKE values in the stagnation region decrease. As regards the effects of the parameter g/w, by decreasing the feedback channel minimum cross-sectional area, the oscillation frequency of the sweeping jet increases, while the amplitude of the jet oscillation decreases.

1. Introduction

Without requiring any moving part or piezoelectrical elements, fluidic oscillators are actuators able to convert a steady jet into an oscillating one, only due to internal fluid dynamic mechanisms. Since the oscillations of such jets are self-induced and self-sustained, the interest in fluidic oscillators has grown over the last years, especially for film cooling (Hossain et al. (2018)), flow control (Koklu & Owens (2017)) and heat transfer applications (Zhou et al. (2019)). Three main categories of fluidic oscillators are suggested in the literature: feedback-free oscillators, oscillators with one feedback channel and oscillators with two feedback channels. The latter design is the one investigated in the current study. The oscillation frequency, the sweeping angle and the flow field characteristics

of sweeping jets greatly depend on various geometric and fluid dynamic parameters. Therefore, in the current work, through the application of the planar PIV technique, the effects of nozzle-to-plate distance and feedback channel minimum cross-sectional area on the external flow field of impinging sweeping jets are investigated.

2. Experimental setup and procedure

Figure 1 illustrates a sketch of the employed experimental setup (left) and of the fluidic oscillator (right).

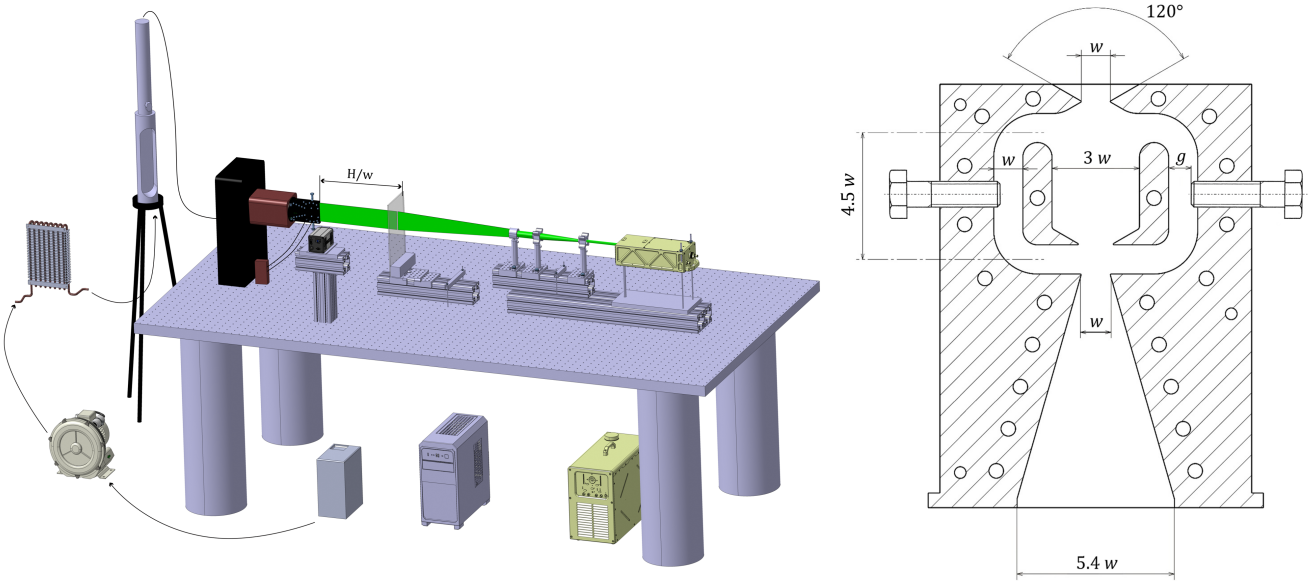

Figure 1. Sketch of the experimental setup (left) and of the fluidic oscillator (right).

A centrifugal blower is employed to collect air from the ambient and a heat exchanger is used to keep the air temperature equal to the ambient one. The air flow passes through a plenum chamber and then through the fluidic oscillator, to finally impinge on a transparent glass panel, which is mounted on a translation stage that allows the variation of the nozzle-to-plate distance H/w. The flow is seeded with $1\mu m$ diameter olive oil particles, generated by a Laskin nozzle. A $1\ mm$ thick laser sheet passes through the impinging plate and illuminates the symmetry plane of the fluidic oscillator. The external flow field of a two feedback channels fluidic oscillator is analysed; in order to investigate the effects of the feedback channel minimum cross-sectional area, the device is provided with threaded holes in correspondence of the feedback channels, in which a screw is fastened to vary the parameter g/w, representing the ratio between the feedback channel minimum passage width g and the exit nozzle throat width w, chosen as reference length. In the current investigation the value of the Reynolds number is set at 1.7×10^4 and the following values of

H/w and g/w are considered: $H/w = 2, 4, 6, 8, 10$ and $g/w = 0.17, 0.33, 0.50, 0.67, 1$. Time-averaged and phase-averaged analyses are performed; indeed, the pressure signal measured between the inlet and outlet sections of one feedback channel is used to identify the phase of each velocity snapshot, despite the velocity measurements are not time-resolved.

3. Results

The configuration having $g/w = 1$ is firstly taken as reference case, thus analysing the nozzle-to-plate distance effect. The phase-averaged velocity and fluctuating kinetic energy fields show that the jet sweeps in the external flow field, with a sweeping angle approximately equal to $25°$ and a frequency of 50 Hz. Due to this behaviour, the jet exhibits a twin-jet pattern, which can be identified from both the time-averaged axial velocity and Phase-correlated Kinetic Energy (PKE) (Greco et al. (2017)) distributions (see Figure 2). Indeed, the highest PKE values are obtained in correspondence of the extreme positions reached by the jet in its oscillating motion; such regions are those in which the coherent temporal oscillation of the velocity values is greater and, therefore, the PKE values are the greatest. Moreover, high PKE values are reached in proximity of the impingement plate, due to a strong variation of the crosswise velocity component.

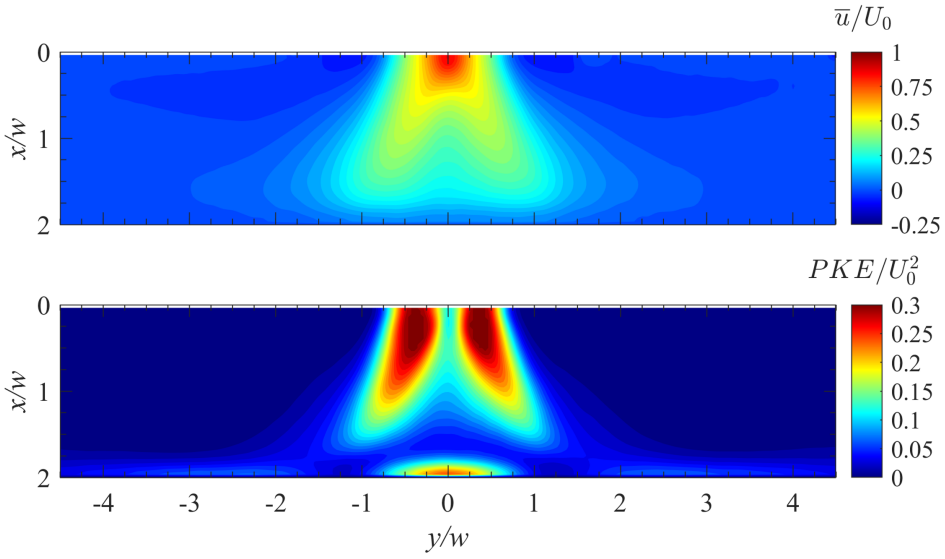

Figure 2. Dimensionless time-averaged axial velocity and PKE fields, $H/w = 2$, $g/w = 1$.

Figure 3 illustrates the dimensionless phase-averaged axial velocity and fluctuating kinetic energy fields at $H/w = 2$, for the configuration having $g/w = 1$. Three equally spaced phase angles ranging between $\phi = 0°$ and $\phi = 180°$ are depicted, being $\phi = 0°$ the phase in which the jet reaches the left extreme position in the external flow field. As it is possible to observe from Figure 3, the jet sweeps in a rigid-like way from the left to the right side in the external flow field. Further-

more, a head vortex which follows the motion of the jet, thus moving along the impinging plate, is identifiable; such phenomenon has also been observed by Woszidlo et al. (2015). Additionally, it is possible to highlight that the dimensionless phase-averaged axial velocity distribution is not symmetrical with respect to the jet centreline; indeed, the region of the highest values of the dimensionless phase-averaged axial velocity is shifted towards the x-axis (i.e. $y/w = 0$) during each phase of the sweeping motion. This phenomenon influences the dimensionless fluctuating kinetic energy distributions, thus determining greater values of the latter in the right shear layer while the jet moves from the left to the right side of the external flow field; this behaviour reverses once the jet reaches the right extreme position in the external flow field and, afterwards, moves to the left again.

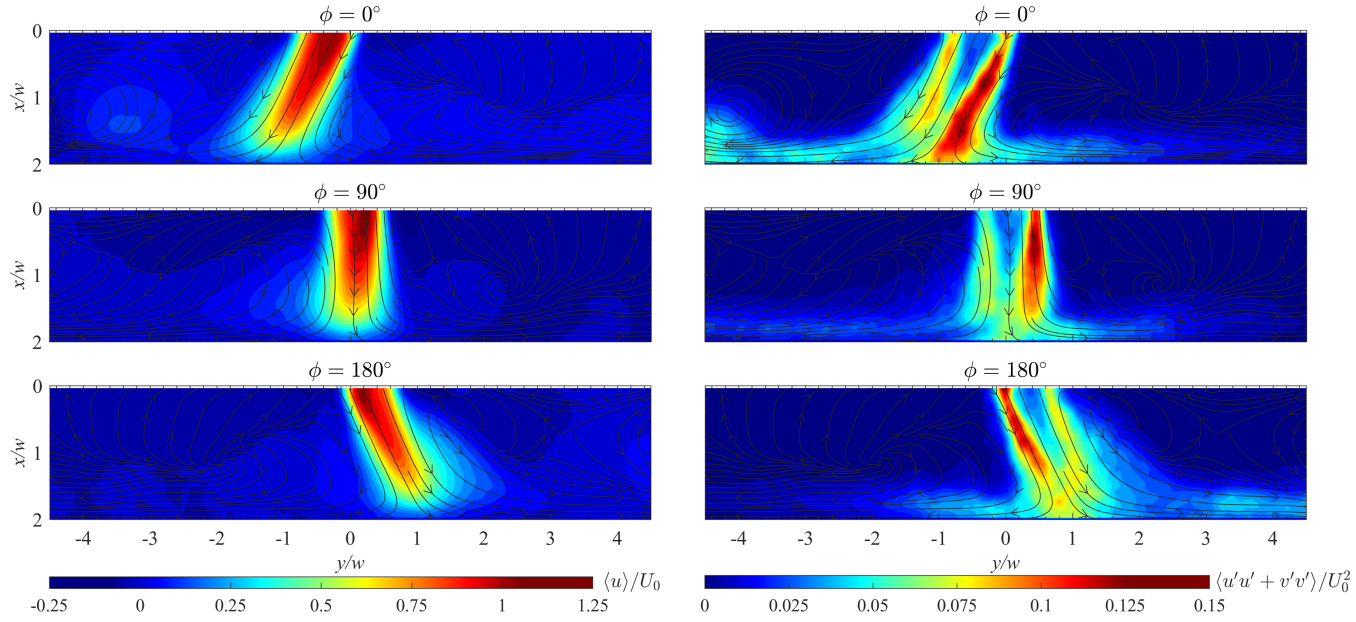

Figure 3. Dimensionless phase-averaged axial velocity fields (left) and fluctuating kinetic energy fields (right), $H/w = 2$, $g/w = 1$.

In Figure 4 the dimensionless time-averaged axial velocity and PKE fields are depicted for the configuration having $g/w = 1$ and at $H/w = 8$. A twin-jet pattern is still identifiable in the external flow field, being the values of the time-averaged axial velocity and PKE greater in correspondence of the most deflected positions of the jet. Nevertheless, by comparing the time-averaged PKE field obtained at $H/w = 8$ (Figure 4) with the corresponding one obtained at $H/w = 2$ (Figure 2), it is possible to observe that at $H/w = 8$ the values of the PKE in proximity of the impingement plate are lower than those obtained at $H/w = 2$, due to the increase of the nozzle-to-plate distance.

The dimensionless phase-averaged axial velocity fields and the corresponding dimensionless fluctuating kinetic energy fields are shown in Figure 5 at three phase angles (i.e. $\phi = 0°$, $\phi = 90°$ and $\phi = 180°$). As it can be observed from the comparison of Figure 3 and Figure 5, while at $H/w = 2$ the jet sweeps in an almost rigid-like way between the two extreme positions reached

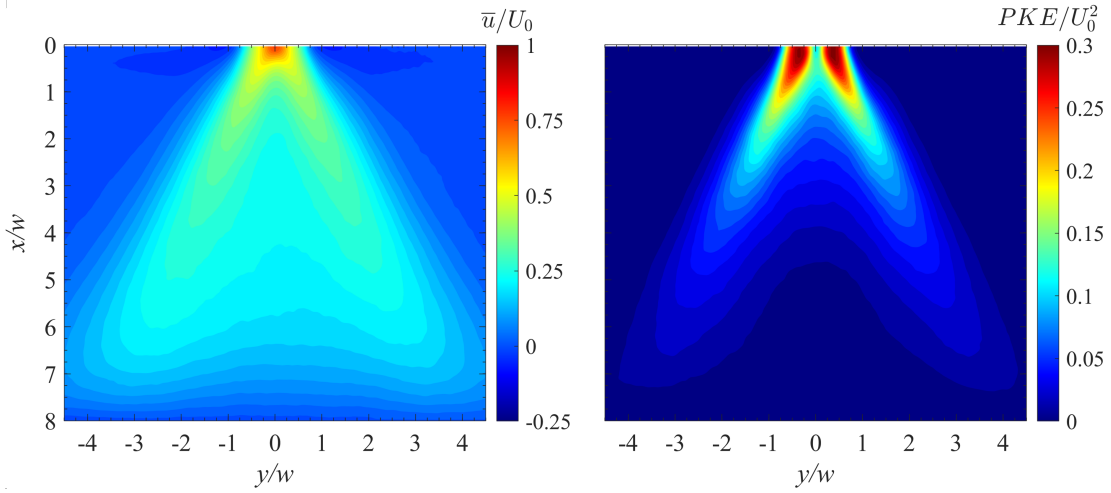

Figure 4. Dimensionless time-averaged axial velocity and PKE fields, $H/w = 8$, $g/w = 1$.

during its oscillating motion (see Figure 3), at greater nozzle-to-plate distances a phase delay between the motion of the jet near the impinging plate and near the exit nozzle section is identifiable (see Figure 5). Furthermore, at larger nozzle-to-plate distances the jet spreading is greater while the impinging streamwise velocities are smaller. It is also remarkable that, as previously seen at $H/w = 2$ (see Figure 3), also at $H/w = 8$ during each phase of the sweeping motion of the jet the region of highest values of the dimensionless axial velocity is shifted towards the x-axis, therefore determining greater values of the dimensionless fluctuating kinetic energy along the right shear layer as the jet is moving from the left to the right side of the external flow field; this phenomenon reverses as the jet reaches the right extreme position, i.e. during the second half of the oscillation cycle.

As regards the effects of the g/w parameter, by reducing the feedback channel minimum cross-sectional area the sweeping angle of the jet decreases, while the oscillation frequency increases. Still, a twin-jet pattern can be identified for $g/w \geq 0.33$, as it can be seen from the crosswise profiles of the dimensionless time-averaged axial velocity (see Figure 6), while the configuration having $g/w = 0.17$ exhibits a single-jet velocity structure. Indeed, as g/w decreases, the maximum values of the axial velocity along the jet centreline increase while the oscillation intensity decreases, resulting in a decrease of the PKE values. These latter phenomena are clearly observable from the analysis of the time-averaged axial velocity and PKE fields for $g/w < 1$. In particular, the comparison of the time-averaged axial velocity and PKE fields at $H/w = 2$ for the configuration having $g/w = 0.33$ (see Figure 7) with the ones obtained at the same nozzle-to-plate distance for $g/w = 1$ (see Figure 2) shows that by reducing g/w the dimensionless axial velocity assumes greater values along the jet centreline, while the values of the PKE decrease and the region of the highest PKE values tends to move towards the x-axis, due to the decrease of the spatial oscillation of the jet.

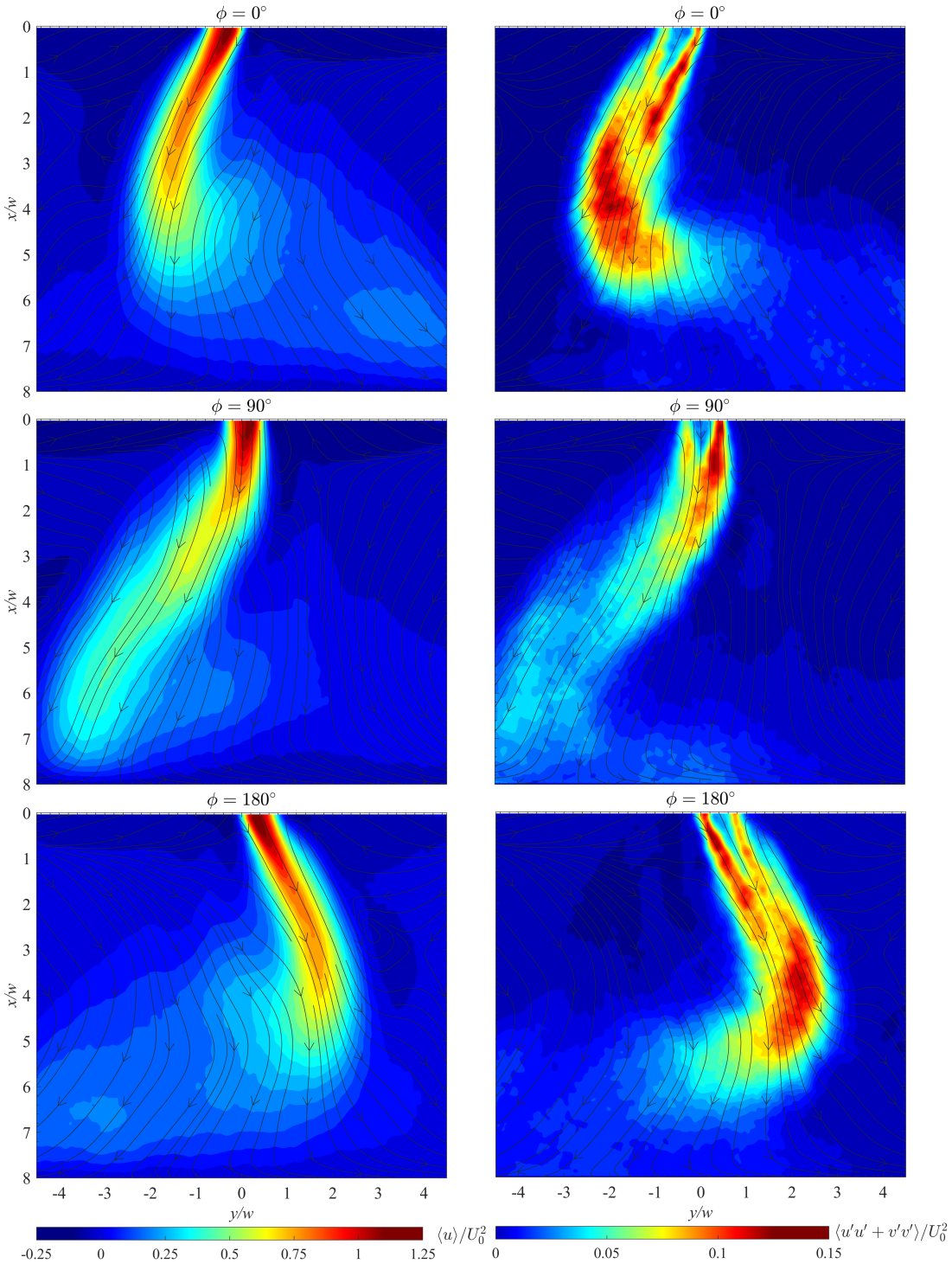

Figure 5. Dimensionless phase-averaged axial velocity fields (left) and fluctuating kinetic energy fields (right), $H/w = 8$, $g/w = 1$.

4. Conclusions

The current study has analysed the effects of nozzle-to-plate distance and feedback channel minimum cross-sectional area on the external flow field of impinging sweeping jets. Values of the non-

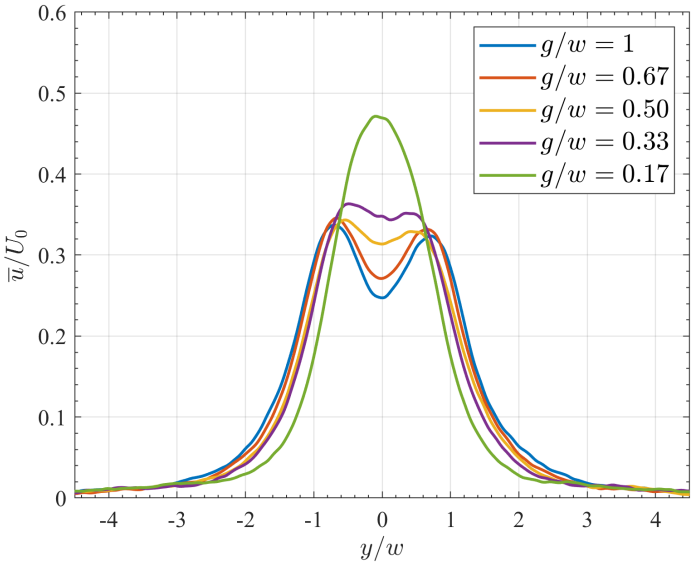

Figure 6. Crosswise profile of the dimensionless time-averaged axial velocity at $x/w = 1.5$ and $H/w = 2$, for $g/w = 1, 0.67, 0.50, 0.33$ and 0.17.

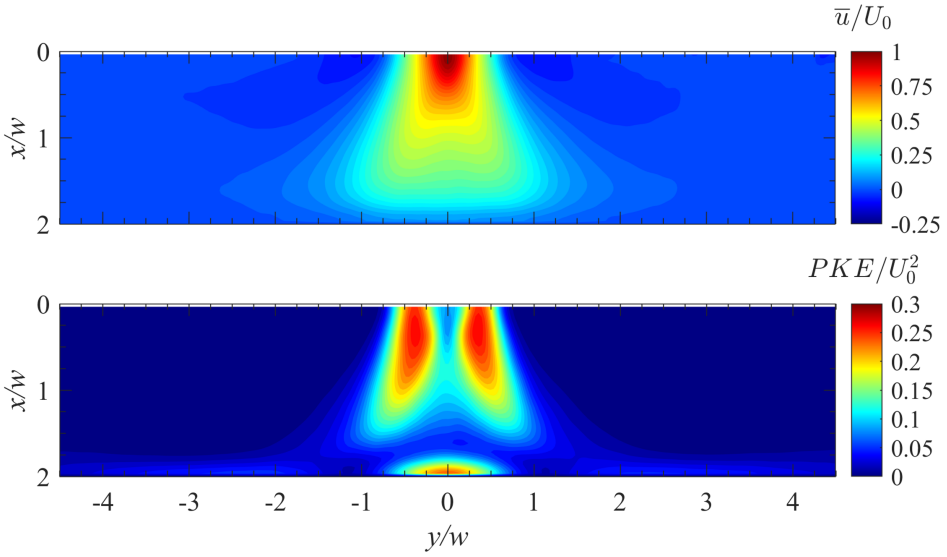

Figure 7. Dimensionless time-averaged axial velocity and PKE fields, $H/w = 2$, $g/w = 0.33$.

dimensional nozzle-to-plate distance H/w ranging between 2 and 10, with a spacing of 2, have been considered. Moreover, the feedback channel geometry has been varied to analyse the effects of the parameter g/w; five different values of the latter have been investigated: $g/w = 0.17, 0.33, 0.50, 0.67$ and 1. The results obtained show that with the increase of the nozzle-to-plate distance the jet no longer sweeps in a rigid-like way from one side to the other, while with the reduction of the feedback channel minimum cross-sectional area the oscillation frequency increases and the sweeping angle decreases.

References

Greco, C. S., Cardone, G., & Soria, J. (2017). On the behaviour of impinging zero-net-mass-flux jets. *Journal of fluid mechanics*, *810*, 25–59.

Hossain, M. A., Prenter, R., Lundgreen, R. K., Ameri, A., Gregory, J. W., & Bons, J. P. (2018). Experimental and numerical investigation of sweeping jet film cooling. *Journal of Turbomachinery*, *140*(3).

Koklu, M., & Owens, L. R. (2017). Comparison of sweeping jet actuators with different flow-control techniques for flow-separation control. *AIAA Journal*, *55*(3), 848–860.

Woszidlo, R., Ostermann, F., Nayeri, C. N., & Paschereit, C. O. (2015). The time-resolved natural flow field of a fluidic oscillator. *Experiments in Fluids*, *56*(6), 1–12.

Zhou, W., Yuan, L., Liu, Y., Peng, D., & Wen, X. (2019). Heat transfer of a sweeping jet impinging at narrow spacings. *Experimental Thermal and Fluid Science*, *103*, 89–98.